Available online at www.sciencedirect.com
ScienceDirect
European Polymer Journal 43 (2007) 1154–1167
EUROPEAN POLYMER JOURNAL
www.elsevier.com/locate/europolj

Macromolecular Nanotechnology

Solvent effects on jet evolution during electrospinning of semi-dilute polystyrene solutions

Goki Eda, James Liu, Satya Shivkumar *

Department of Mechanical Engineering, Worcester Polytechnic Institute, 100 Institute Road, Worcester, MA 01609, USA

Received 26 January 2006; received in revised form 22 December 2006; accepted 2 January 2007
Available online 13 January 2007

Abstract

Linear polystyrene with a weight average molecular weight of 393,400 g/mol was used with various solvents including tetrahydrofuran (THF), chloroform, carbon disulfide (CS_2), 1-methyl-2-pyrrolidinone (NMP), and *N*,*N*-dimethylformamide (DMF) to produce solutions, corresponding to a Berry number of about 9. The jet breakdown behavior of each of these solutions was studied with a high speed camera (2000 frames/s). The structure of the electrospun polymer was examined with a scanning electron microscope. The results indicate that jet breakdown with THF and chloroform entailed significant extensional flow, followed by the onset of instabilities, leading to the formation of numerous secondary jets under steady-state conditions. By comparison, the solution jets with DMF and NMP exhibit extensive whipping and splaying to produce a cloud of jets. In this case, few secondary jets were observed under steady-state conditions. A highly refined structure was observed in the electrospun polymer for NMP and DMF, in accordance with the extensive instabilities observed during jet breakdown. Limited jet instability observed with CS_2 solution suggests the significant effect of solvent evaporation. Typical primary jet velocities were measured to be on the order of 2–5 m/s.

Keywords: Polymer; Polystyrene; Electrospinning; Solvents

1. Introduction

During electrospinning, various physical phenomena occur as the electrostatically driven jet of polymer solution travels across the electric field established between the capillary and the target. This process is initiated as a jet of solution breaks out of the conically protruded pendant drop known as the Taylor cone [1]. The ejected viscoelastic jet is driven towards the target, undergoing extensional flow. Subsequently, a repulsive Coulombic force in the jet results in bending instability and causes lateral perturbations to grow [2]. A high repulsive force in a thin jet may also cause splaying or splitting, resulting in further thinning of the jet [3,4]. Micro- to nanometer scale fibers and beads of various morphologies may be produced as a consequence of repeated jet thinning. The principal features of this process have been summarized in a recent review [5].

The structures produced during electrospinning can consist of beads, fibers, or a combination of

* Corresponding author. Tel.: +1 508 831 5048; fax: +1 508 831 5178.
E-mail address: shivkuma@wpi.edu (S. Shivkumar).

0014-3057/$ - see front matter © 2007 Elsevier Ltd. All rights reserved.
doi:10.1016/j.eurpolymj.2007.01.003

the two, often referred to as bead-on-string structures [6,7]. Several investigators have shown that a bead to fiber transition may occur as the molecular weight and/or the concentration of the polymer in solution is increased [8–10]. Stable fibers may be produced when sufficient chain entanglements are present in the solution [10,11].

The overall morphology of the electrospun polymer is strongly influenced by the physical and electrical properties of the solution, determined to a large extent by the type of solvent [7,12]. For example, it has been reported that solvents with high dielectric constant typically result in finer and more uniform fibers in the electrospun polymer [12–16]. The development of the structure in the polymer obtained on the collector and the corresponding role of the solvent has not been clearly understood. Koombhongse et al. [4] have shown that jet instabilities developing at the Taylor cone may be influenced by the type of solvent used for the spinning process. Their results indicate that the characteristics of the fibers in the structure obtained on the collector may depend on the extent of bending instability, splaying and splitting. The development of these jet instabilities is a complex phenomenon that is controlled by several factors including solution rheology, charge density, surface tension and solvent evaporation rate [17,18]. Previous study has shown that polymer concentration as well as molecular weight influences the development of jet instabilities and the resulting microstructure [19]. Since the morphology of electrospun fibers depends on various solvent properties, the jet breakdown behavior may be unique to a specific polymer-solvent system. The purpose of this work is to study the jet evolution with polystyrene with various solvents by utilizing a high speed camera. Experiments have been conducted with moderate to good solvents, with widely varying dielectric constant and evaporation rates.

2. Experimental procedure

Linear polystyrene with a weight average molecular weight (M_w) of 393,400 g/mol and polydispersity of 1.16 (Scientific Polymer Products, Ontario, NY) was dissolved in various solvents (reagent grade) shown in Table 1. The concentration of polymer was adjusted such that the Berry number, $[\eta]C$, was around 9 ($[\eta]$ is the intrinsic viscosity and C is the concentration) [20]. The concentration was calculated according to:

$$C\ (\mathrm{g/mol}) = \frac{9}{[\eta]} = \frac{9}{KM_w^a} \quad (1)$$

where K and a are the Mark–Houwink constants based on the polymer, solvent and temperature [21]. The values of K and a for different solvents are listed in Table 2 [22–24]. The Mark–Houwink constants for most of the solvents used in this study were readily available for most solvents, typically obtainable from many sources. These constants (Table 2) were used in Eq. (1) to calculate the concentration of the polymer. The Mark–Houwink constants for the polystyrene-CS_2 system, however, were not readily available. Consequently, experiments with CS_2 were conducted at the same concentration as that of THF (Table 2). Based on the only available source for the Mark–Houwink constant for this system [24], the approximate $[\eta]C$ for this condition was calculated to be 7.5. It should be noted that CS_2 was selected as solvent because of its extremely high vaporization rate compared to the other solvents used in the study. Approximately 0.04–0.06 g of polymer was dissolved in 0.5 mL of solvent to achieve the desired solution concentration (Table 2). No filtration process was utilized due to the high purity of the polymer. The solution was obtained in a 1 mL syringe equipped with an 18 gauge needle (inner diameter = 0.84, 51 mm long). The syringe was placed horizontally on a syringe

Table 1
Solvents used in this study

Solvent	Supplier	bp (°C)	ΔH_v (kJ mol^{-1})	ε	$\eta \times 10^3$ (kg m^{-1} s^{-1})	$\gamma \times 10^2$ (N m^{-1})
Tetrahydrofuran	Sigma–Aldrich	66	32.0	7.58	0.46	2.64
Chloroform	Alfa Aesar	61	33.3	4.81	0.536	2.653
N,*N*-Dimethylformamide	Sigma	153	47.5	36.71	0.802	3.642
1-Methyl-2-pyrrolidinone	Sigma–Aldrich	202	52.8	32.20	1.67	4.07
Carbon disulfide	Sigma–Aldrich	46	27.5	2.64	0.363	3.225

Relevant properties of the solvent including boiling point (bp), heat of vaporization (ΔH_v), dielectric constant (ε), viscosity (η) and surface tension (γ) are also shown [31].

Table 2
Mark–Houwink constants for the solvents used in this study

Solvent	$K \times 10^3$ (mL/g)	a	T (°C)	Reference	C (g/mL)	$[\eta]$ (mL/g)	$[\eta]C$
Tetrahydrofuran	11	0.725	25	[22]	0.072	125	9.0
Chloroform	7.16	0.76	25	[22]	0.070	128	8.9
N,*N*-Dimethylformamide	31.8	0.603	35	[22]	0.120	75	9.0
1-Methyl-2-pyrrolidinone	12	0.72	85	[23]	0.071	128	9.2
Carbon disulfide	3.46	0.8	25	[24]	0.072	104	7.5

The temperature, T, at which the data have been reported, is indicated. The concentration of polymer used in the experiment (C), the intrinsic viscosity $[\eta]$ and the corresponding Berry number ($[\eta]C$) are also shown. Polystyrene with a weight average molecular weight (M_w) of 393,400 g/mol was used in all the experiments.

pump (EW-74900-00, Cole-Parmer) as shown in Fig. 1. A grounded aluminum foil collector (10 cm × 10 cm) was positioned 10 cm from the tip of the needle. The pump was calibrated to achieve a flow rate of 3 mL/h for all experiments. A potential of 30 kV was applied to the needle immediately after a pendant drop formed at the tip. All electro- spinning processes were conducted in ambient air at room temperature. A high speed camera (Phantom V.5.1., Vision Research) equipped with Nikon 150 mm lens was used to capture the solution jet images at a rate of 2000 frames per second with exposure time of 259 μs. The images were extracted and analyzed using the proprietary software (Cine-View606) supplied by Vision Research. The morphology of the electrospun fibers was examined with a scanning electron microscope (JSM-840) after sputter-coating the sample with gold–palladium.

3. Results and discussion

The rheology of polymer solutions has a significant effect on the morphology of electrospun fibers [10,25,26]. The interaction of polymer molecules in solution can be described in terms of C^*, the dilute solution limit at which the hydrodynamic volumes of the dissolved molecules begin to overlap, and C_e, the entanglement concentration [10]. The concentration C_e can be considered to be a crossover from a concentration range where intramolecular excluded-volume effects control the solution viscosity to a regime where intermolecular entanglements begin to have a significant effect on the rheological properties of the solution. When the concentration is increased beyond C_e, the zero shear viscosity shows a steep increase due to the extensive entanglements of the polymer chains. It has been reported that during electrospinning, stable fibers can be

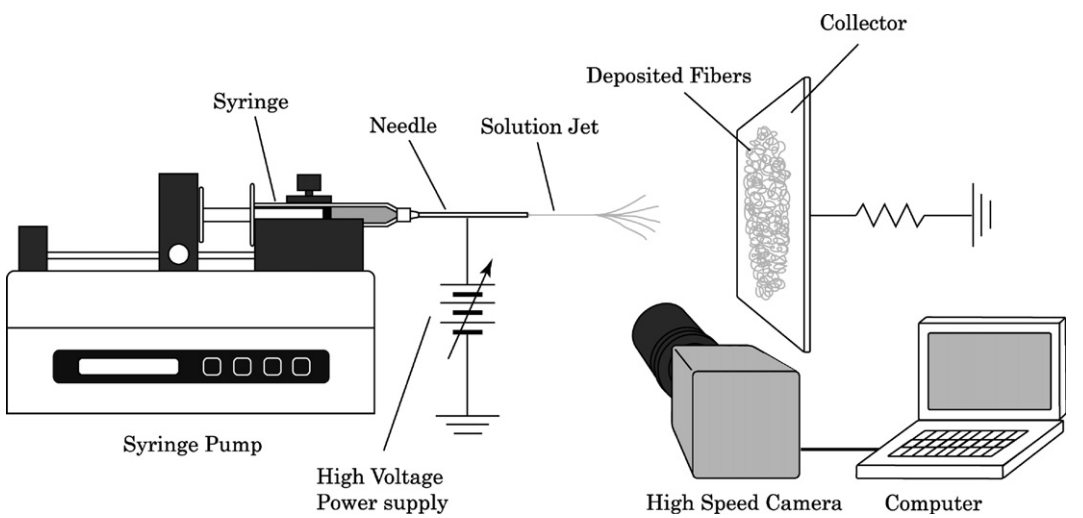

Fig. 1. Schematic of the experimental set-up.

formed with solutions in this regime, i.e. $C > C_e$ [10]. Shenoy et al. [11] proposed that the transition from bead-only to a bead-on-string structure occurs at a concentration corresponding to one entanglement per chain. The degree of chain overlap can also be expressed in terms of the Berry number, $[\eta]C$ [20]. For polystyrene with a $M_w = 390{,}000$ g/ml in a good solvent such as tetrahydrofuran (THF), C_e has been measured to be around 0.06 g/ml [27], which corresponds to $[\eta]C$ value of 7.8. Lee et al. [28] have electrospun polystyrene with THF as the solvent for a solution concentration equivalent to $[\eta]C$ of about 8. The morphology consisted of beaded fibers and half hollow spheres. Megelski et al. [9] have produced polystyrene fibers with THF as the solvent for a range of concentration equivalent to $[\eta]C$ of 14–35. They obtained a bead-on-string structure at $[\eta]C$ of 14 and a fully fibrous structure at $[\eta]C$ of 35. These results suggest that there is a general agreement with the theory in terms of entanglement concentration and fiber formation. For polystyrene-THF system in this study, the minimum concentration at which some stable fibers were observed corresponded to $[\eta]C$ of 9.

Photographs showing the structure in the electrospun polymer are shown in Fig. 2 for various solvents used in this study. When THF, chloroform, or carbon disulfide (CS_2) were used as solvents, the structure consisted of fine fibers, cups and dimpled beads, typically on the order of 10–20 μm, similar to the data of Lee et al. [28]. The morphology obtained with 1-methyl-2-pyrrolidinone (NMP) solution consisted of a number of beads, which were much smaller in size (1–5 μm) compared to those obtained with THF, chloroform, and CS_2 (Fig. 2d). Some fibers connecting these beads were also observed indicating that the solution concentration was in the transition regime. The fine structure obtained with NMP implies the high charge density achieved resulting from repeated breakdown of solution jet. In contrast to these bead dominant morphologies, a highly fibrous structure was obtained with *N*,*N*-dimethylformamide (DMF) solution indicating that the transition from bead

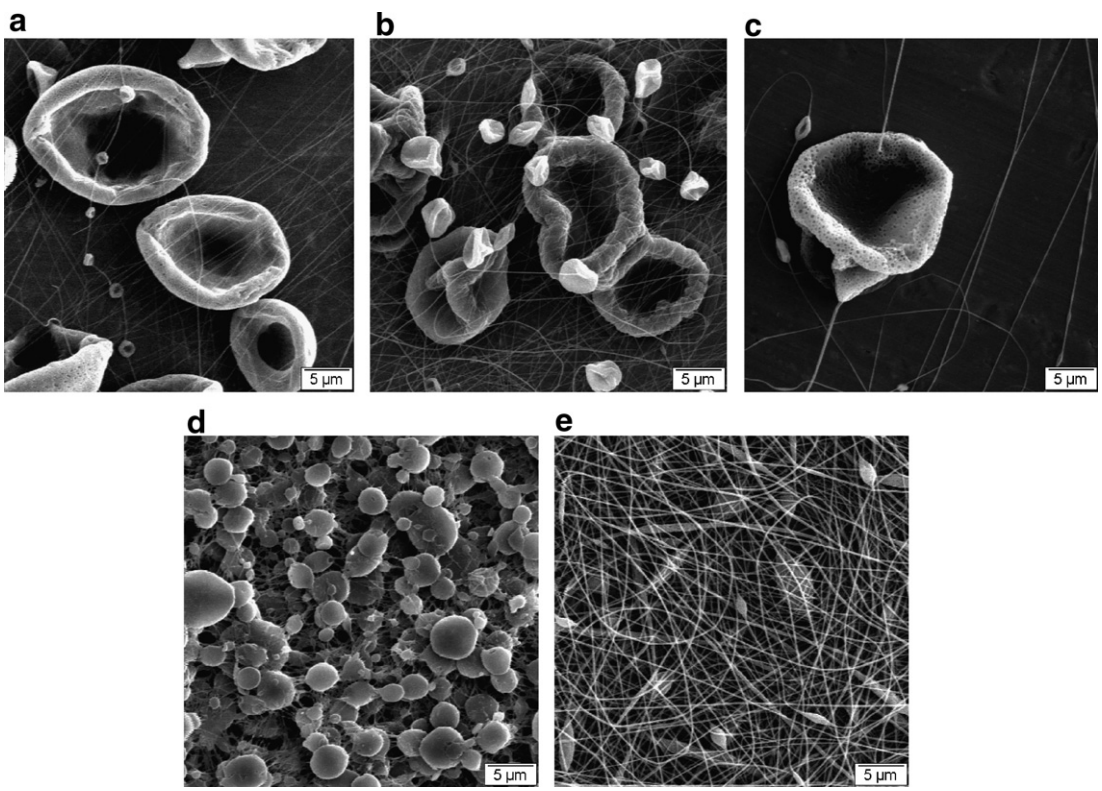

Fig. 2. SEM photographs of polystyrene fibers and beads electrospun with various solvents (a: THF, b: Chloroform, c: CS_2, d: NMP, e: DMF).

to fiber may occur with smaller degree of chain overlap (Fig. 2e).

The development of the solution jet during electrospinning involved various stages with all solvents examined in this study. The process generally begins with the formation of the primary jet, followed by the evolution of the jet due to jet instabilities. After some time, the process eventually stabilizes with a steady-state profile. Despite the chaotic nature of electrospinning, the phenomena observed at different stages were reproducible and unique in each solvent.

Various stages in the development of the jet as the solution emerges from the capillary are shown in Fig. 3 for THF. The ejected jet of solution underwent an extensional flow for the first few milliseconds after jet initiation and traveled in a straight line for a distance of about 25 mm from the capillary. Subsequently, about 7 ms after jet initiation, the tip of the jet broke down into a number of beads, which are seen as bright segments in Fig. 3. The beads are seen as bright segments due to their high velocity. The formation of beads indicates insufficient chain entanglement. However, because the solution concentration is in the entanglement regime, it can be expected that these beads may be connected by thin fibers that are not visible in the photograph. It is likely that bead formation was triggered by bending instability at the tip of the jet. About 11 ms after jet initiation, small perturbations

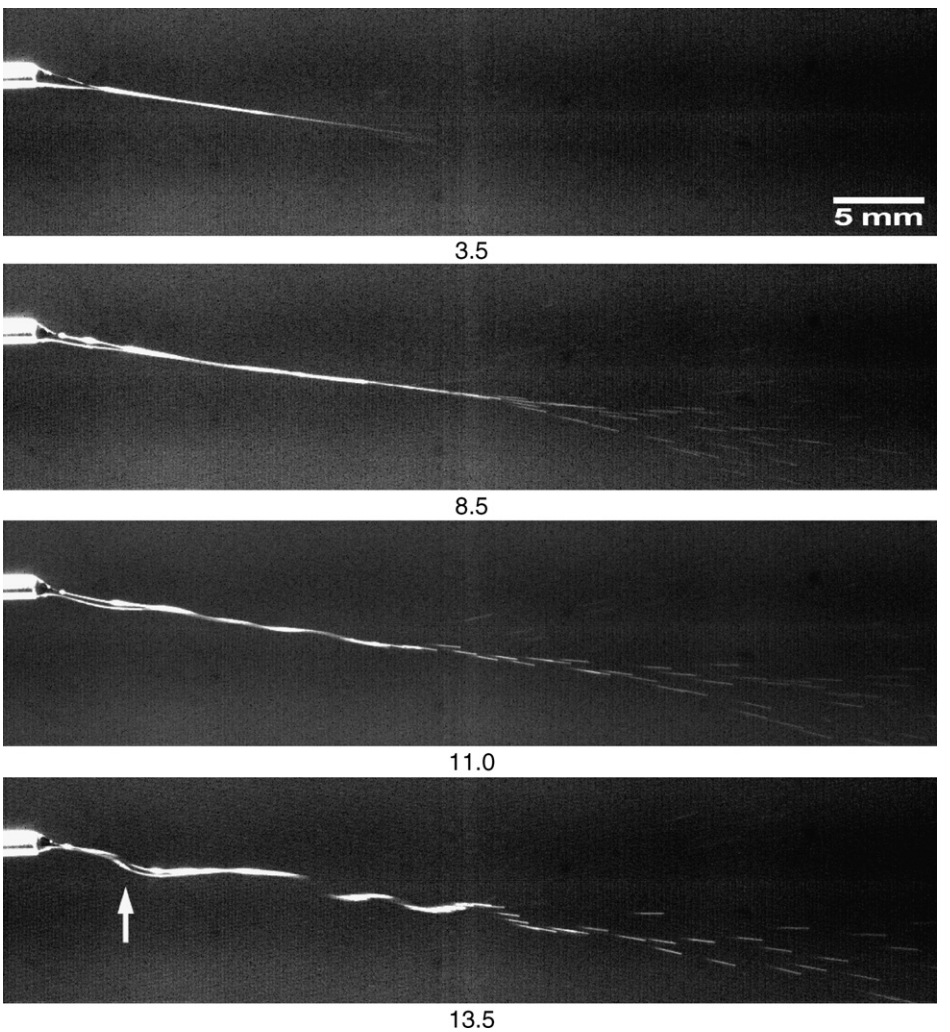

Fig. 3. Sequential photographs showing the initial development of instabilities in the primary jet emerging from the capillary. The segment indicated by the arrow develops further jet instability shown in Fig. 4. The numbers indicate the time elapsed (ms) after the jet emerges from the Taylor cone (solvent: THF, $C = 0.072$ g/mL).

along the jet became large, yielding a wave-like profile (Fig. 3). The perturbation indicated by the arrow in Fig. 3 gradually grew into the bent jets shown in Fig. 4. This bending may have been caused not only by the electrical force but also by the buckling in the segment. In this case, the compressive force may have resulted because the thick segment of the jet (indicated by the arrow in Fig. 3) advanced relatively slowly compared to the fresh jet ejected from the capillary. The arrow in Fig. 4 indicates the looping of the jet, which was observed in more detail with back scattered lighting as shown in Fig. 5a. This loop of jet eventually breaks down into beads as discussed above. The back scattered photographs show that as the jet of THF solution flowed out of the initial drop, the surface of the Taylor cone receded to the capillary tip. Subsequently, a secondary jet appeared from the edge of the capillary as shown in Fig. 5b. This secondary jet was observed typically 20–30 ms after primary jet initiation. The bending instability of the primary jet became less intensive after the emergence of the secondary jet and, subsequently, these jets essentially became indistinguishable (Fig. 5b and c). Several jets appeared in a similar fashion from the capillary end one after another until a pseudo-steady state was reached (Fig. 6). At this stage, the Taylor cone was no longer observable suggesting that it had moved inside the capillary, as has been reported previously [6,29]. Numerous steady-state minijets were ejected in the radial direction from the edge of the capillary. It is likely that these minijets were ejected towards the direction where the electric field was the strongest. The development of bending instability at the end of each of the minijets can also be seen in Fig. 6 (similar to the looping in the secondary jet observed in Fig. 5c). A photograph of the needle tip after electrospinning, highlighting solidified fibers is shown in Fig. 7. The direction of the solidified fibers matches the profile observed during steady-state flow (Fig. 6). The photograph shown in Fig. 7 also indicates the complex nature of jet instability.

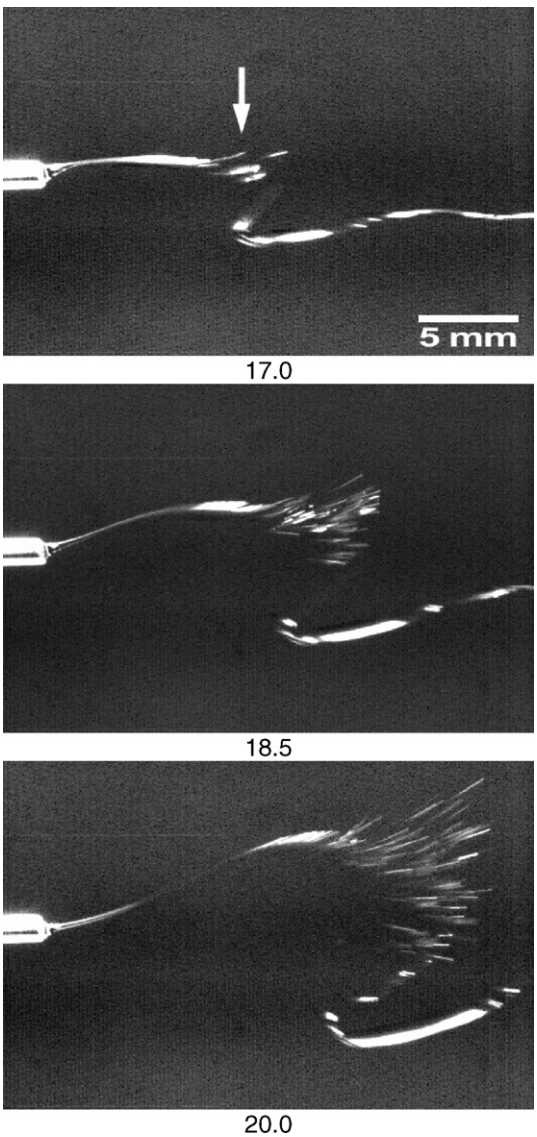

Fig. 4. Images showing a growing perturbation leading to the breakup of the primary jet. The arrow indicates the loops created due to bending instability. The numbers indicate the time elapsed (ms) after the jet emerged from the Taylor cone (solvent: THF, $C = 0.072$ g/mL).

A similar trend in jet evolution was observed when chloroform was used as the solvent as shown in Fig. 8. The primary jet underwent elongational flow for the initial few milliseconds after it emerged from the Taylor cone. Bending instability was observed in both the primary and the secondary jet, as was the case for THF solution. The perturbations in the primary jet grew considerably and eventually enabled the jet to break down into beads in a manner similar to that observed with THF solution (Fig. 8c). As the Taylor cone receded to the capillary, secondary jets were ejected one after another from the edge of the capillary until a steady-state profile was observed (Fig. 8d). This steady-state was reached about 40 ms after jet initiation.

The jet breakdown observed with DMF as the solvent was significantly different from either THF or chloroform. In this case, a jet of solution was ejected from the Taylor cone and immediately

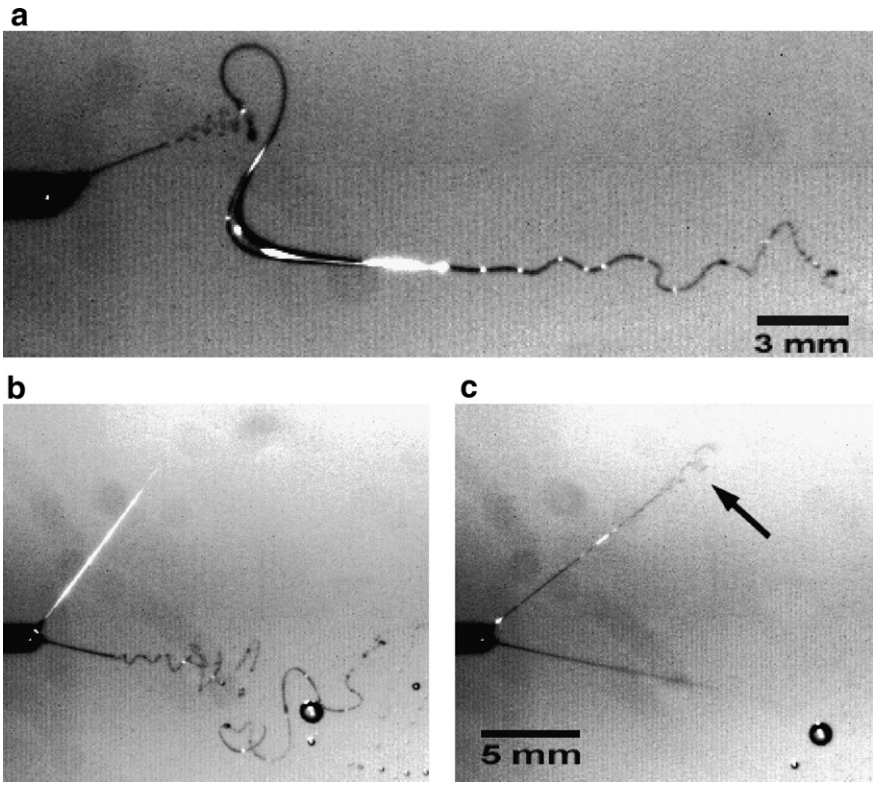

Fig. 5. Photographs showing: (a) the primary jet undergoing bending instability; (b) the development of a secondary jet and (c) bending instability in the secondary jet (indicated by the arrow). The time elapsed (after the primary jet emerges from the Taylor cone) for the formation of the secondary jet is typically on the order of 20 ms (solvent: THF, $C = 0.078$ g/mL).

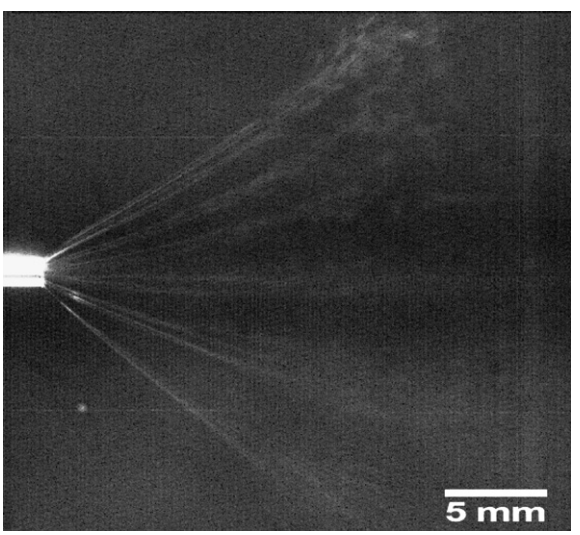

Fig. 6. Photograph showing numerous minijets emerging from the capillary under steady-state conditions. The time elapsed after the initial jet emerged from the Taylor cone is 43.5 ms (solvent: THF, $C = 0.072$ g/mL).

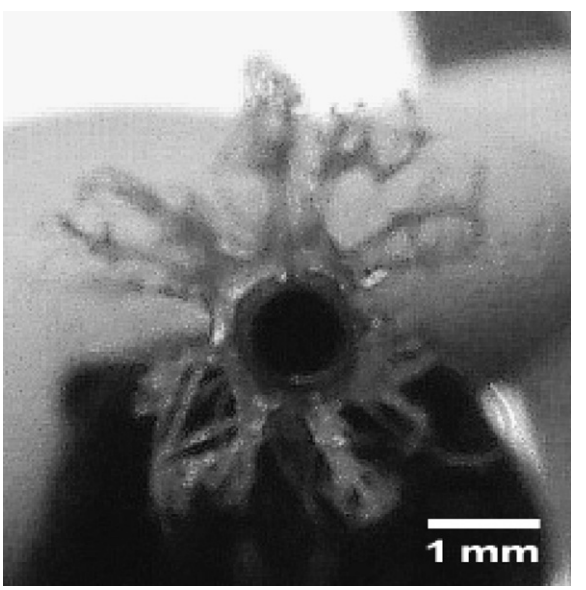

Fig. 7. Photograph showing the tip of the needle at the end of the experiment. Numerous solidified fibers can be observed in the radial direction around the capillary edge (solvent: THF, $C = 0.072$ g/mL).

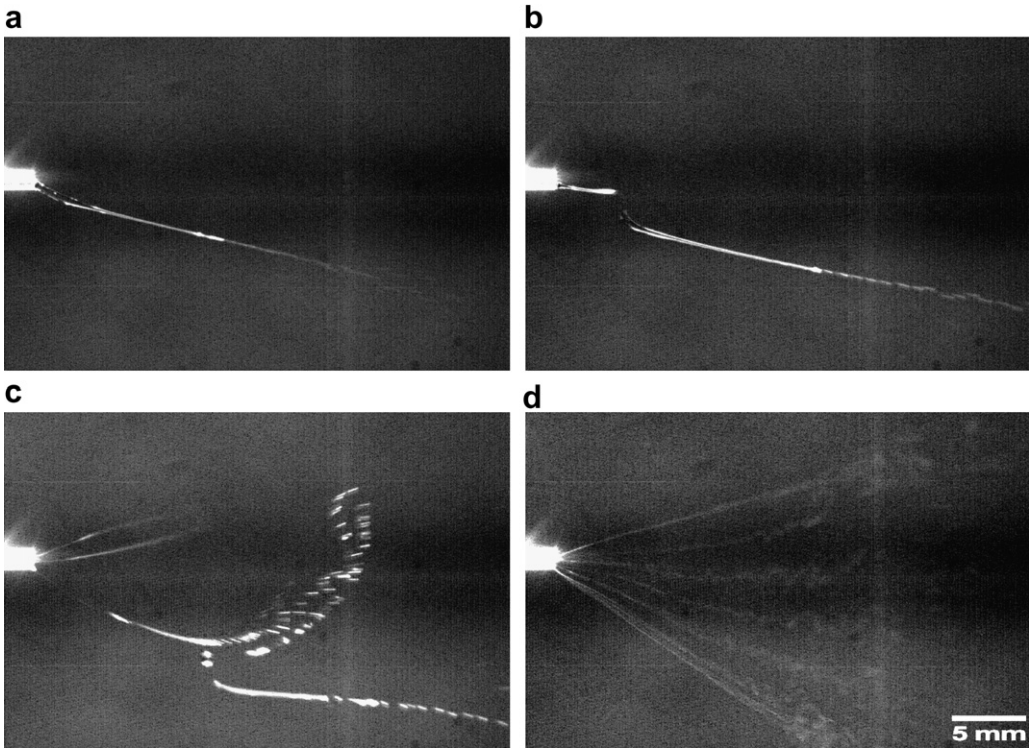

Fig. 8. Photographs showing the jet development and breakdown during electrospinning with chloroform as the solvent: (a) elongational flow; (b) development of bending instability; (c) breakup of primary jet and emergence of secondary jets, and (d) numerous jets under steady state ($C = 0.070$ g/mL).

formed a cloud of jet a few millimeters away from the Taylor cone as shown in Fig. 9. This cloud may consist of jets undergoing splaying and whipping at a high frequency. The lateral size of the cloud grew for a few milliseconds and remained constant about 8 ms after jet initiation. The breakup of the jet indicates that the electrical force due to the charges in the jet became large enough to overcome the surface tension and the viscoelastic force of the solution. It can be expected that the relatively high dielectric constant and the polyelectrolyte behavior of DMF may promote a high charge density in the jet. A similar discussion about the effect of DMF has been reported previously [10–15]. The surface tension of DMF is slightly larger than that of THF or chloroform, which implies that a larger force is required to cause bending and splaying. The immediate breakup of the jet, therefore, suggests that the charge density within the jet of DMF solution was significantly higher than that in THF and chloroform solution. As the jet progressed, an oscillation was observed in the cloud of jet (Fig. 9). The oscillation of the cloud eventually evolved into a spiral, in a manner much similar to the development of bending instability of a single jet. This phenomenon was reported by Reneker et al. [30] for polycaprolactone in acetone. Reneker et al. [30] measured the length of the straight segment of the jet before the onset of instability to be around 3 mm, which is comparable to the value obtained in this study with DMF solution (although the electric field strengths are different in these experiments). During jet evolution, a change in the shape of the Taylor cone was often observed as shown in Fig. 9. This change may be due to the balancing of the excess charge accumulated in the Taylor cone and the charge that is dispensed together with the jet. It was often observed that when the Taylor cone was in a conical shape, the breakup of the jet was more significant and occurred closer to the Taylor cone, suggesting a variation of charge density within the jet.

The jet of DMF solution underwent a series of chaotic events before reaching a steady state. Sequential photographs demonstrating secondary jet development and jet splitting are shown in

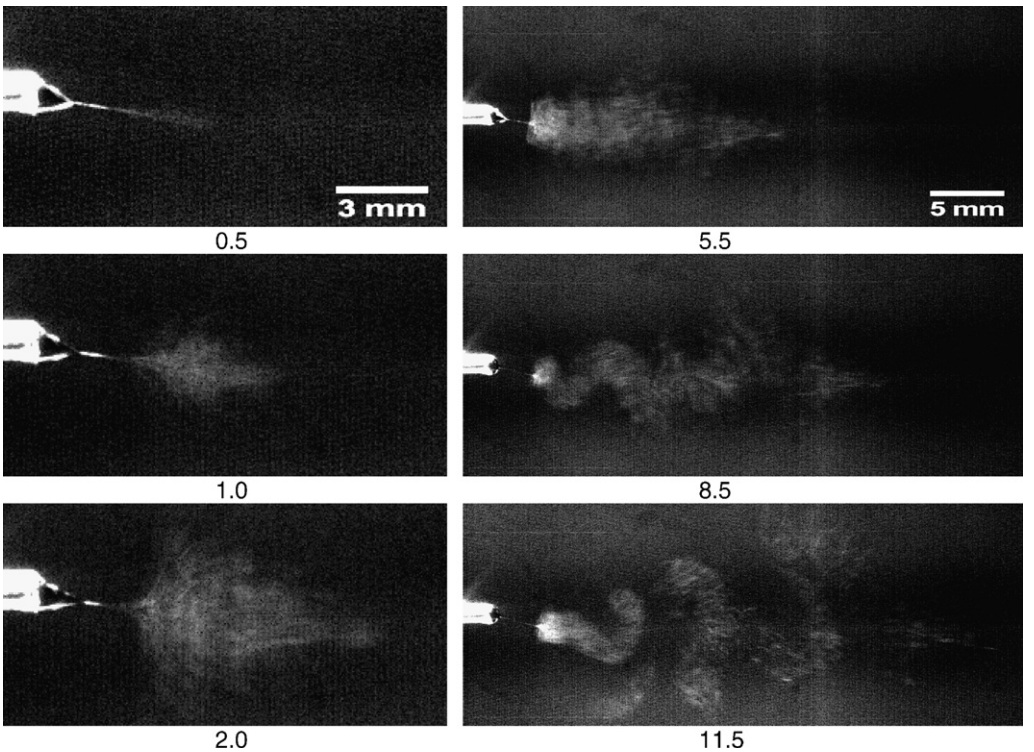

Fig. 9. Sequential photographs showing morphological changes in the primary jet during electrospinning with DMF as the solvent. The numbers indicate the time elapsed (ms) after the jet emerged from the Taylor cone. Note the oscillations in the primary jet after 5.5 ms ($C = 0.120$ g/mL).

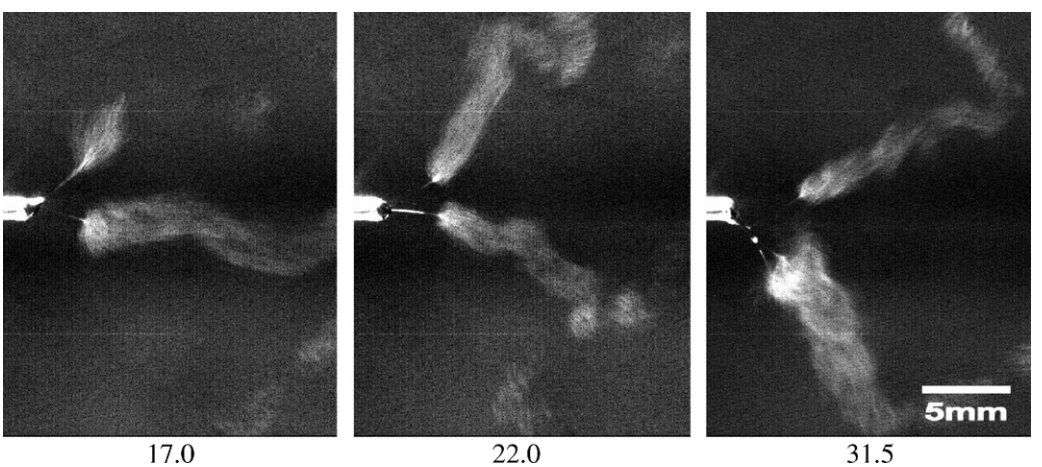

Fig. 10. Photographs showing the development and breakdown of the secondary jet during electrospinning with DMF as the solvent. The numbers indicate the time elapsed (ms) after the jet emerges from the Taylor cone ($C = 0.120$ g/mL).

Fig. 10. The secondary jet appeared and developed a whipping motion in a similar fashion as the primary jet. During the secondary jet formation, the vertex of the Taylor cone directed towards the emerging secondary jet, suggesting the inequality in the charges distributed to the two jets. Subsequently, the development of a large perturbation in the Taylor cone resulted in splitting of a jet (Fig. 10). The jets that formed at this stage were extremely unstable and showed extensive whipping as seen in the

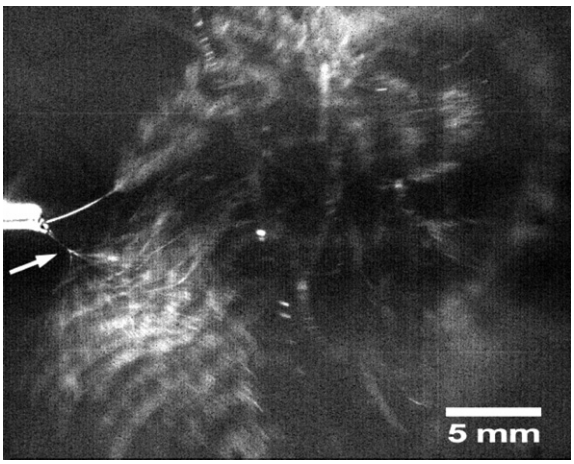

Fig. 11. Photograph showing examples of extremely chaotic jets that undergo extensive splitting and whipping during electrospinning with DMF as the solvent. Such chaotic events are typically observed before a steady-state pattern develops ($C = 0.120$ g/mL).

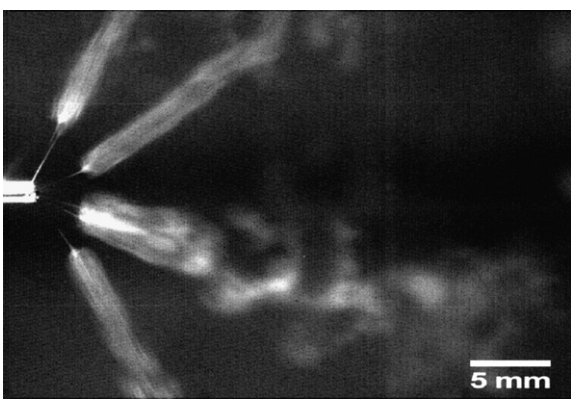

Fig. 12. Photograph showing several jets emerging from the capillary under steady-state conditions during electrospinning with DMF as the solvent. The time elapsed after the initial jet emerged from the Taylor cone is 181.5 ms ($C = 0.120$ g/mL).

lower jet (indicated by the arrow) in Fig. 11. These instabilities continued for about 100 ms and eventually, a steady-state profile was reached as shown in Fig. 12. Unlike the case of THF and chloroform, the Taylor cone is still observable at this stage with DMF solution. Five steady-state jets can be seen to break down into clouds of jet approximately equal distance from the capillary tip. The lateral sizes of the jet cloud are also approximately equal.

The jet evolution observed with NMP as the solvent showed a trend similar to that of DMF solution. The ejected jet of NMP solution immediately broke down into a cloud of jet as shown in Fig. 13. Splaying of jet was frequently observed for a few milliseconds after the formation of a jet. The occurrence of the splaying coincided with the meniscus attaining a conical shape as opposed to hemispherical shape, indicating the presence of high excess charge within the Taylor cone. The lateral size of the cloud grew larger and more diffuse compared to DMF solutions suggesting that the jet broke down into a number of beads as was observed in the microstructure (Fig. 2). After jet initiation, various unstable events followed and continued until a steady-state was reached. Elongation of the Taylor cone, formation of a secondary jet, and splitting and merging of two jets were frequently observed in this stage (Fig. 13). The steady-state profile was reached typically about 160 ms after jet initiation. The Taylor cone was observed outside the capillary at this stage. Fig. 14 shows five jets breaking down into a cloud of jets. The cloud of jets did not exhibit a whipping motion unlike the DMF solution, suggesting highly dispersed charges in the space.

The jet evolution with CS_2 as the solvent showed a different behavior compared to the previous solvents, as shown in Fig. 15. After the formation of the Taylor cone, small droplets were ejected from the vertex. While the droplets were ejected, the Taylor cone was stretched towards the collector and Rayleigh instability caused this elongated Taylor cone to break into droplets. This breakup continued until a fresh Taylor cone was formed and a stable jet was ejected. This late formation and the singularity of the stable jet is possibly due to the extremely low boiling point of CS_2, which may have resulted in the formation of skin on the surface of the initial Taylor cone. The stable jet exhibited some degree of instability as indicated by the arrow in Fig. 15, however, it remained as a single straight jet most of the time. After about 40 ms of steady jet observation, the Taylor cone began to stretch as in the preliminary stage of jet formation and this process was repeated.

The transient jet velocity of each solution immediately after jet initiation was measured. In each frame following jet initiation, position of the jet was recorded by marking the tip of the jet. In the case of DMF and NMP solution, the position at the tip of the jet cloud was recorded. The average velocity of the jet between two successive frames was thus calculated for each solution. The variation of the jet velocity with the time elapsed after jet initiation is plotted in Fig. 16. The jet velocity of THF,

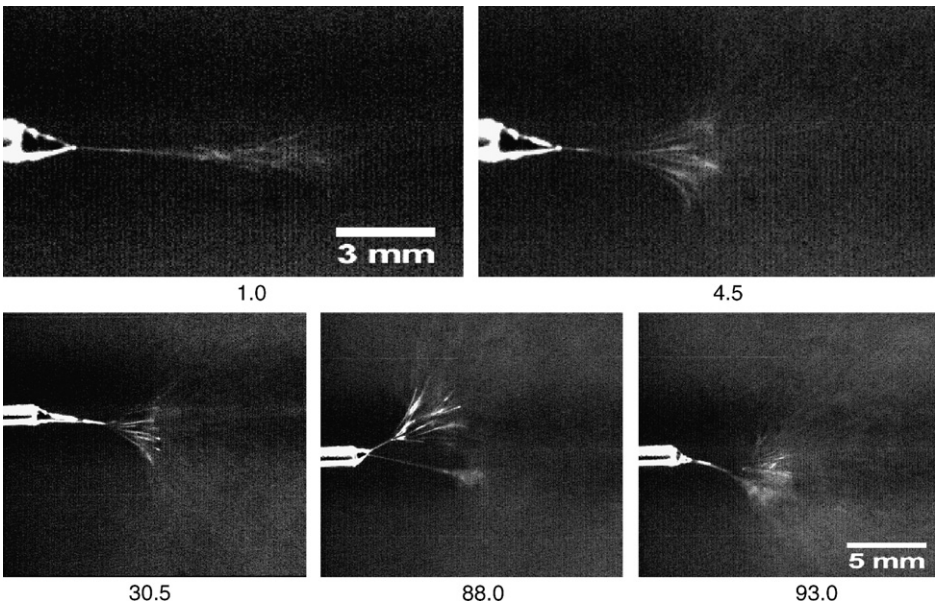

Fig. 13. Photographs showing the jet breakdown during electrospinning with NMP as the solvent. The numbers indicate the time elapsed (ms) after the jet emerges from the Taylor cone ($C = 0.071$ g/mL).

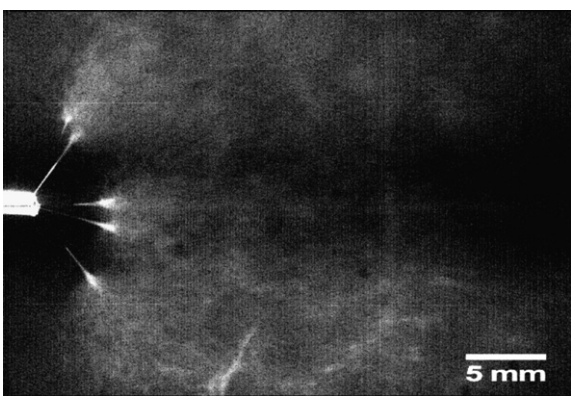

Fig. 14. Photograph showing several jets emerging from the capillary under steady-state conditions during electrospinning with DMF as the solvent. The time elapsed after the initial jet emerged from the Taylor cone is 161 ms ($C = 0.071$ g/mL).

chloroform, and CS_2 solution was found to be relatively constant during the observed time interval. The constant jet velocity suggests that equilibrium is established between the electrical force pulling the jet towards the collector and the resisting viscoelastic force. On the other hand, DMF and NMP solutions exhibited a dramatic decrease in velocity in the first 2 ms after jet initiation. This deceleration coincides with the jet breakup, which DMF and NMP solutions undergo immediately after jet initiation (Figs. 9 and 13). The complex trajectory within the jet cloud may have resulted in the reduction of velocity. The velocity of the jet reported by Reneker et al. [30] for the polycaprolactone–acetone system is about 0.7 m/s. By comparison, steady-state primary jet velocities in this study were generally between 2 and 5 m/s (Fig. 16).

It was observed that the overall jet evolution and breakdown can be grouped into two categories as shown in Fig. 17. The jet evolution observed with the first group of solvents, THF and chloroform, can be characterized by high degree of extensional flow, limited instability, and a large number of secondary jets. The jet evolution of this group of solvents involved a large bending of the primary jet, followed by the emergence of the secondary jets. On the other hand, DMF and NMP solutions exhibited a limited extensional flow, high degree of instability, and a small number of secondary jets. CS_2 was not included in either of the categories. The various instability phenomena observed with DMF and NMP suggest that the electric properties of the solution play a dominant role in structure formation.

Bending instability of an electrified jet causes small perturbations along the jet to grow as they travel towards the collector. Because the position at which this perturbation starts to grow and its growth rate are relatively constant for a given condition, a jet of solution undergoing bending instability

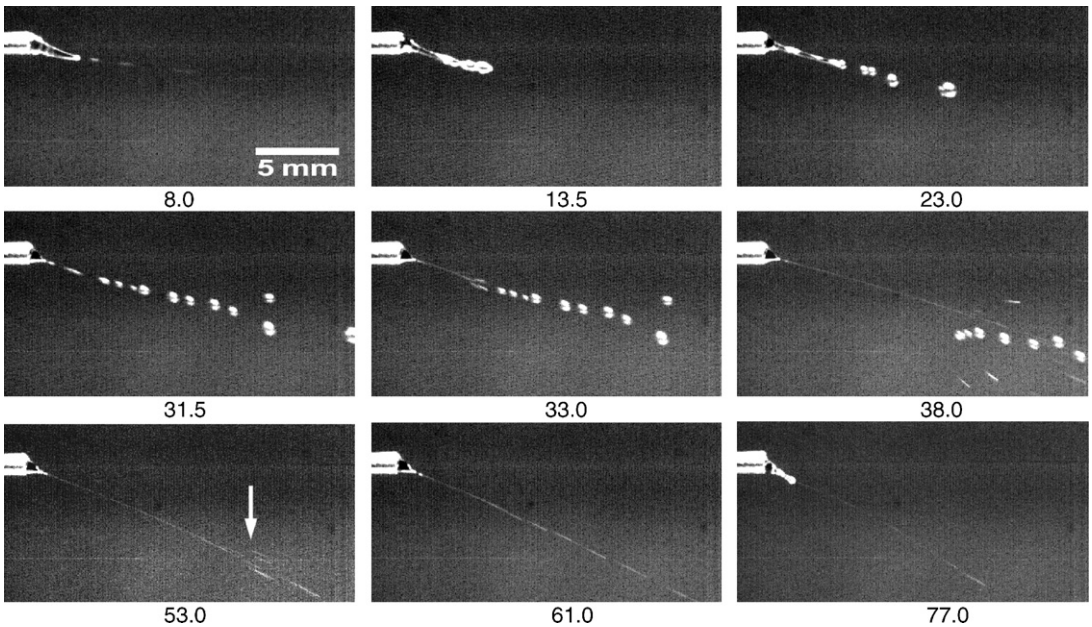

Fig. 15. Photographs showing the jet breakdown during electrospinning with CS_2 as the solvent. The numbers indicate the time elapsed (ms) after the initial droplet emerges from the Taylor cone. The arrow indicates the breakup of a single steady state jet ($C = 0.072$ g/mL).

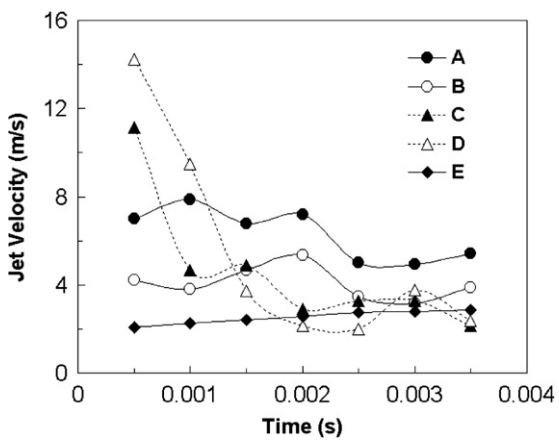

Fig. 16. Jet velocity as a function of time for various solvents. The time was measured after a stable jet emerged from Taylor cone. The typical standard deviation was around ±2 m/s (A: THF, B: chloroform, C: DMF, D: NMP, E: CS_2).

typically produces a shape referred to as an envelope cone [18]. The shape and the size of the envelope cone are determined by various factors such as the initial charge density, surface tension and the viscoelastic properties of the solution. The observation of envelope cone shape is important because it is related to the draw ratio of the jet, as has been described by Yarin et al. [18]. In this experiment, a stable cone was observed for all the solutions except for CS_2. In these solutions, a stable cone was observed in the early stage of the primary jet development and in secondary jets. The size of the envelope cone was measured from photographs in which a stable cone could be observed. An example of this envelope cone is shown in Fig. 3. The jet breaks into a number of beads, which together form a cone shape with its vertex lying at the end of the extensional flow. The radius of the cone was measured and plotted as a function of the distance from the capillary tip as shown in Fig. 18. It is clearly seen that the development of instability is much more rapid and occurs earlier for DMF and NMP solutions compared to THF and chloroform solutions. This trend is observed for both the primary and the secondary jets indicating the presence of high charge density in these jets. The reasons for the differences observed in the envelope cone shape between the DMF and NMP solution are not readily evident; however, it is likely that the NMP solution did not have sufficient viscosity and broke down into beads immediately after the initial whipping of jet as speculated from the microstructure (Fig. 2). Another factor determining the envelope cone shape is the evaporation of the solvent. Yarin et al. [18] theoretically determined the radius of the envelope cone and found that when the evaporation of the solvent is not taken into account in the calculation, the radius of

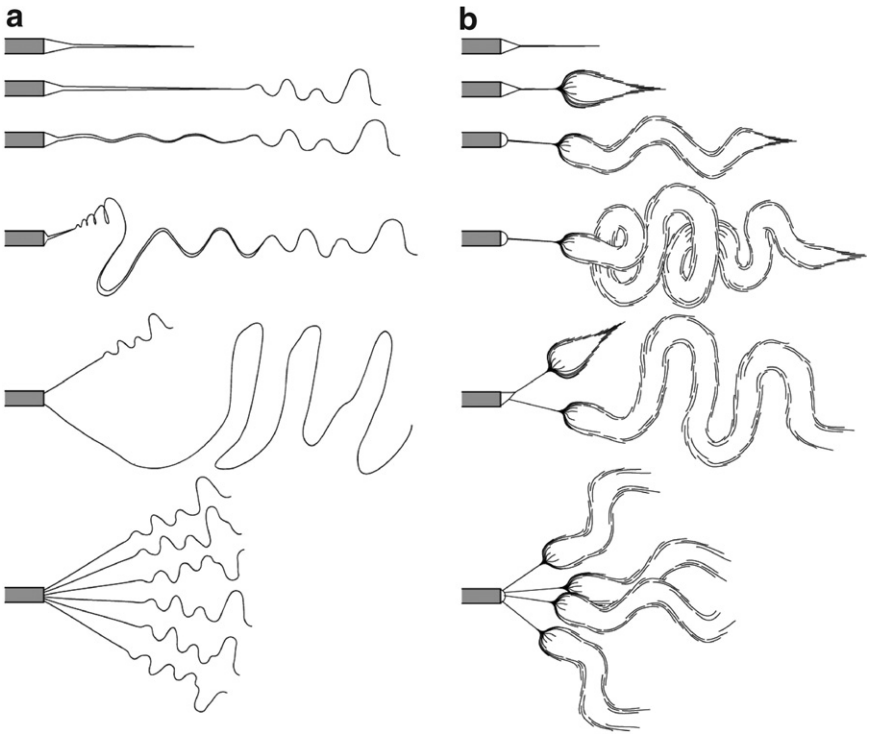

Fig. 17. Schematic of jet breakdown exhibited by two groups of solvent.

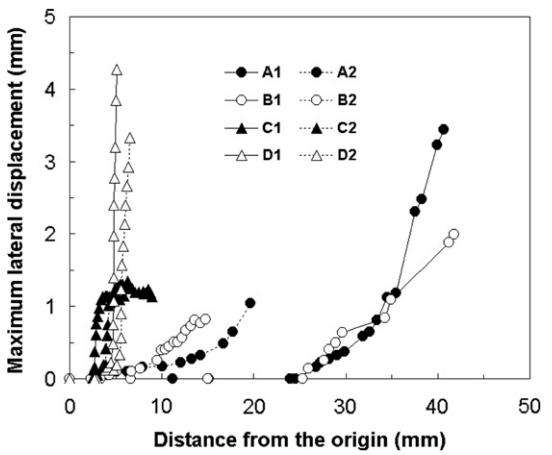

Fig. 18. Maximum size of the envelope cone formed during jet instability measured from a photograph (A: THF, B: chloroform, C: DMF, D: NMP). Numbers 1 and 2 indicate primary and secondary jet, respectively.

the envelope cone grew more rapidly compared to their experimental data. As evaporation and solidification take place, viscosity and elastic modulus of the jet increase dramatically, leading to a slow stretching of the jet. The fact that no stable cone was formed with CS_2 implies that the effect of evaporation was significant. An increased jet stiffness resulting from rapid solidification may have suppressed bending instability. However, solvent evaporation rate and electrical properties should not be considered independently because instability phenomena increase the jet surface area where solvent can evaporate.

4. Conclusions

Solvents used for electrospinning have a major effect on the various physical phenomena occurring during the formation and disintegration of the jets emerging from the Taylor cone. Some solvent properties such as dielectric constant and evaporation rate were found to play a dominant role in determining the behavior of the solution jet during the process. For solutions in the transition regime between beads and beaded fibers, two classes of solvents were identified based on the development of jet instabilities. The first class of solvents is characterized by large extensional flow, limited degree of instability, and a large number of the secondary jets that form under steady-state conditions. In this case, the primary jet velocity is relatively constant

(3–4 m/s). THF and chloroform are examples of this type of behavior. In solvents with a high dielectric constant such as DMF and NMP, the jet breakdown occurs through repeated whipping and splaying to produce a cloud of jets. In this case, there was a reduction in jet velocity after the onset of bending and whipping instabilities. Steady-state velocities, however, were comparable to the value obtained with THF and chloroform. The rapid skin formation with highly volatile solvents such as CS_2 may inhibit the development of jet instabilities and thereby minimize the formation of secondary jets. The structure in the electrospun polymer was similar for THF, chloroform and CS_2 and consisted of fine fibers, cups and dimpled beads, typically on the order of 10–20 μm. In the case of DMF and NMP, the beads and fibers were highly refined (~1–5 μm) confirming the extensive instabilities the solution experiences during electrospinning.

References

[1] Taylor GI. Proc Roy Soc Lond A 1969:313–453.
[2] Reneker DH, Yarin AL, Fong H, Koombhongse S. J Appl Phys 2000;87:4531.
[3] Reneker DH, Chun I. Nanotechnology 1996;7:216–23.
[4] Koombhongse S, Liu W, Reneker DH. J Polym Sci Part B: Polym Phys 2001;39:2598–606.
[5] Subbiah T, Bhat GS, Tock RW, Parameswaran S, Ramkumar SS. J Appl Polym Sci 2005;96:557–69.
[6] Deitzel JM, Kleinmeyer J, Harris D, Tan NCB. Polymer 2001;42:261–72.
[7] Fong H, Chun I, Reneker DH. Polymer 1999;40:4585–92.
[8] Zong X, Kim K, Fang D, Ran S, Hsiao BS, Chu B. Polymer 2002;43:4403–12.
[9] Megelski S, Stephens JS, Rabolt JF, Chase DB. Macromolecules 2002;35:8456–66.
[10] Gupta P, Elkins C, Long TE, Wilkes GL. Polymer 2005;46:4799–810.
[11] Shenoy SL, Bates WD, Frisch HL, Wnek GE. Polymer 2005;46:3372–84.
[12] Son WK, Youk JH, Lee TS, Park WH. Polymer 2004;45:2959–66.
[13] Lee KH, Kim HY, La YM, Lee DR, Sung NH. J Polym Sci Part B: Polym Phys 2002;40:2259–68.
[14] Lee KH, Kim HY, Khil MS, Ra YM, Lee DR. Polymer 2003;44:1287–94.
[15] Hsu CM, Shivkumar S. Macromol Mater Eng 2004;289:334–40.
[16] Yang Q, Zhenyu LI, Hong Y, Zhao Y, Qiu S, Wang CE, et al. J Polym Sci Part B: Polym Phys 2004;42:3721–6.
[17] Hohman MM, Shin M, Rutledge G, Brenner MP. Phys Fluids 2001;13:2201–20.
[18] Yarin AL, Koombhongse S, Reneker DH. J Appl Phys 2001;90:4836.
[19] Eda G, Liu J, Shivkumar S. Mater Lett [in press].
[20] Hager BL, Berry GC. J Polym Sci Polym Phys Ed 1982;20:911–28.
[21] Sperling LH. Introduction to physical polymer science. 2nd ed. NewYork: Wiley; 1992.
[22] Brandrup J, Immergut EH, Grulke EA. Polymer handbook. 4th ed. New York: Wiley; 1999.
[23] Peureux JM, Lochon P. Eur Polym J 1983;19:565–74.
[24] Gan YSJ, Nuffer R, Guenet JM, Francois J. Polym Commun 1986;27:233–5.
[25] Koski A, Yim K, Shivkumar S. Mater Lett 2004;58:493–7.
[26] McKee MG, Wilkes GL, Colby RH, Long TE. Macromolecules 2004;37:1760–7.
[27] Jamieson AM, Telford D. Macromolecules 1982;15:1329.
[28] Lee KH, Kim HY, Bang HJ, Jung YH, Lee SG. Polymer 2003;44:4029–34.
[29] Shin YM, Hohman MM, Brenner MP, Rutledge GC. Polymer 2001;42:9955–67.
[30] Reneker DH, Kataphinan W, Theron A, Zussman E, Yarin AL. Polymer 2002;43:6785–94.
[31] Riddick JA, Bunger WB, Sakano TK, Weissberger A. Organic solvents: physical properties and methods of purification. Techniques of chemistry, vol. 2. NewYork: Wiley; 1986.